Internal Dielectric Transduction in Bulk-Mode Resonators

Dana Weinstein, *Member, IEEE*, and Sunil A. Bhave, *Member, IEEE*

Abstract—This paper investigates electrostatic transduction of a longitudinal-mode silicon acoustic resonator with internal dielectric films. Geometric optimization of internal dielectrically transduced resonators is derived analytically and shown experimentally. Analysis of internal dielectric transduction shows a maximum transduction efficiency with thin dielectric films at points of maximum strain of the desired resonant mode. With this design optimization, a silicon bar resonator is realized with a ninth harmonic resonance of 4.5 GHz and a quality factor of over 11 000, resulting in a record high $f \cdot Q$ product in silicon of 5.1×10^{13}. The novel dielectric transducer demonstrates improved resonator performance with increasing frequency, with optimal transduction efficiency when the acoustic wavelength is twice the dielectric thickness. Such frequency scaling behavior enables the realization of resonators up to the super-high-frequency domain. [2009-0071]

Index Terms—Acoustic transducers, acoustoelectric devices, capacitance transducers, Q-factor, resonators, semiconductor devices.

I. INTRODUCTION

SEMICONDUCTOR electromechanical resonators, with quality factors ($Q's$) often exceeding 10 000, provide a low-power small-footprint CMOS-compatible alternative to various electrical components in wireless communication and signal processing. As the communication industry moves toward quad-band and seven-band technology, there is a growing demand for light-weight low-power compact cell phones that operate at the global range of frequencies. Currently, radio front ends require 10–15 large power-hungry filters fabricated on different substrates using conventional surface acoustic wave or film bulk acoustic resonator (FBAR) technology. However, filter banks composed of high-Q micromechanical filters can be fabricated on-chip in silicon, reducing size, weight, cost, and power in radio communications.

Silicon micromechanical resonators also have promising applications in microprocessor technology. As microprocessors scale to higher frequencies of operation and toward multicore

systems, clocking precision and synchronization at every register becomes increasingly important. High-Q small-footprint CMOS-integrated mechanical resonators can provide synchronized clocking arrays in high-performance microprocessors with reduced power, jitter, and skew.

Extending the frequency of MEMS resonators generally entails scaling of resonator dimensions leading to increased motional impedance. Most electrostatic MEMS resonators to date employ air-gap capacitive transduction to drive and sense a resonant motion. Dielectric electrostatic transduction has several benefits over common air-gap transduction; it is desirable in order to achieve smaller capacitive gaps, to prevent pull-in and stiction symptomatic of air-gap transducers, and to enhance driving force and capacitive sensing due to high dielectric permittivity. Dielectrics can therefore extend resonant frequencies to the > 5 GHz range, where these issues are most prominent. However, most devices demonstrated to date are geometrically identical to their air-gap counterparts, with a dielectric film in place of the air-gap transducer. As resonators scale to higher frequencies and smaller dimensions, this transduction configuration may not be most suitable. This paper focuses on scaling electrostatic acoustic resonators to the super-high-frequency and extremely high frequency (HF) bands of the radio spectrum. Resonator applications in this frequency range include microwave oscillators, with particular emphasis on low-power clocking in microprocessors.

In this paper, we present the highest acoustic frequency measured in silicon resonators to date at 4.51 GHz. We propose and experimentally verify the optimal design for "internal dielectric transduction" of longitudinal bulk-mode MEMS resonators. This transduction mechanism increases in efficiency as the dielectric thickness approaches the acoustic half wavelength in silicon. With dielectric films at positions of maximum strain (minimum displacement) in the resonator, a 4.51 GHz resonator is demonstrated with a 9.8 dB signal enhancement relative to its performance at 1.53 GHz. Our analysis and experimental verification of improved resonator performance at higher frequency promise scaling of MEMS resonators to previously unattainable frequencies.

The underlying difference between "internal" [1] and "external" [2] dielectric transductions determines their capabilities at higher frequencies. Both mechanisms employ dielectric drive and sense transducers. External transduction assumes free boundary conditions (zero stress) at the dielectric interface, driving at a frequency corresponding to a resonant mode with maximum displacement at the dielectric and necessitating maximum acoustic mismatch between the dielectric and resonator bulk. This condition is an extension of the case of air-gap
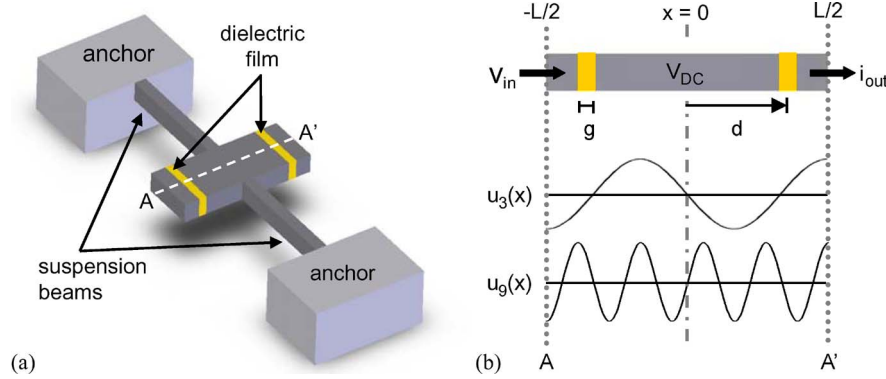
Fig. 1. (a) Schematic of dielectrically transduced free–free longitudinal bulk-mode resonator. The dielectric films are incorporated into the resonator, driving and sensing electrostatically. (b) Cross section of bar resonator. A bias voltage V_{DC} is applied to the resonator. An ac voltage v_{in} on one end drives the resonance, while an output current i_{out} is measured at the other. The normalized amplitudes of the third and ninth longitudinal-mode harmonics are displayed.

transducers, in which the acoustic mismatch approaches infinity in vacuum. The boundary condition at the dielectric interface results in an observed transduction loss, particularly at higher frequencies.

On the other hand, internal transduction incorporates the dielectric film into the resonant mode shape. This generally involves the assumption of a close acoustic match between the bulk resonator and the dielectric film. In practice, a mismatch in acoustic impedance between the dielectric and resonator material results in a shift of the resonant frequency and can easily be compensated by altering the dimensions of the resonator.

II. THEORY

A longitudinal-mode bar resonator is driven and sensed electrostatically with thin vertical dielectric layers, as shown in Fig. 1(a). The resonator body is biased to V_{DC}, and a harmonic excitation of amplitude v_{in} is applied to the drive electrode at resonant frequency. Internal transduction requires that the dielectric films be acoustically matched to the bulk resonator material, thereby maintaining the mode shape and frequency of the resonator without degrading the quality factor. With this assumption, the nth harmonic of the free–free longitudinal mode bar spanning $-L/2 \leq x \leq L/2$ has the following displacement:

$$u(x,t) = U_0 e^{i2\pi \cdot f_n t} \sin(k_n x), \qquad n \text{ odd} \qquad (1)$$

where $k_n = n\pi/L$ and U_0 is the maximum amplitude of vibrations of the bar. Fig. 1(b) shows the third and ninth harmonics of this longitudinal mode. The resonant frequency of the nth harmonic is $f_n = (n/2L)\sqrt{Y/\rho}$, where Y and ρ are the Young's modulus and mass density of the bar, respectively. The driving dielectric film of thickness g is placed at $x = d$ in the resonator. The ac component of the capacitive force across the dielectric of permittivity ε_f is

$$f(x,t) = \frac{\varepsilon_f A}{g^2} V_{DC} v_{in} e^{i2\pi \cdot f_n t} \qquad \forall x \in \left[d - \frac{g}{2}, d + \frac{g}{2} \right]. \quad (2)$$

Given the equation of motion for damped vibrations in a bar [3]

$$\rho A \frac{\partial^2 u(x,t)}{\partial t^2} - bA \frac{\partial^3 u(x,t)}{\partial t \partial x^2} - YA \frac{\partial^2 u(x,t)}{\partial x^2} = \frac{\partial f(x,t)}{\partial x} \quad (3)$$

and substituting (1) into (3), the amplitude of vibrations at resonant frequency is given by

$$U_0 = \frac{2Q\varepsilon_f V_{DC} v_{in}}{n^2 \pi^2 Y} \frac{L}{g^2} \left[\sin\left(k_n d - \frac{k_n g}{2} \right) - \sin\left(k_n d + \frac{k_n g}{2} \right) \right] \quad (4)$$

where Q is the quality factor of the resonator. This resonance is detected by the changing capacitance due to vibrations at the sensing dielectric film

$$
\begin{aligned}
i_{out} &= V_{DC} \frac{dC}{dt} = V_{DC} \frac{dC}{du} \frac{du}{dt} \\
&= \frac{\varepsilon_f V_{DC} A}{g^2} \left[\sin\left(k_n d - \frac{k_n g}{2} \right) \right. \\
&\qquad\qquad \left. - \sin\left(k_n d + \frac{k_n g}{2} \right) \right] \cdot 2\pi \cdot f_n U_0 \\
&= \frac{2Q\varepsilon_f^2 V_{DC}^2 A}{n\pi \sqrt{Y\rho} g^4} \left[\sin\left(k_n d - \frac{k_n g}{2} \right) \right. \\
&\qquad\qquad \left. - \sin\left(k_n d + \frac{k_n g}{2} \right) \right]^2 v_{in} \quad (5)
\end{aligned}
$$

resulting in a motional impedance

$$
\begin{aligned}
R_X &\equiv \frac{v_{in}}{i_{out}} \\
&= \frac{n\pi \sqrt{Y\rho}}{2QA\varepsilon_f^2 V_{DC}^2} \frac{g^4}{\left[\sin(k_n d - k_n g/2) - \sin(k_n d + k_n g/2) \right]^2} \quad (6)
\end{aligned}
$$

simplifying to

$$R_X = \frac{n\pi \sqrt{Y\rho}}{8QA\varepsilon_f^2 V_{DC}^2} \frac{g^4}{\cos^2(k_n d) \sin^2(k_n g/2)}. \quad (7)$$

Equation (7) provides important guidelines for optimizing the performance of bulk-mode resonators using internal dielectric transduction. As expected, the quartic dependence of the motional impedance on dielectric thickness necessitates the thinnest dielectric possible. This is generally limited by fabrication and material properties. Furthermore, this form for the motional impedance, differing from air-gap transduction primarily by the trigonometric terms in the denominator, indicates that the position of both drive and sense dielectric films should be
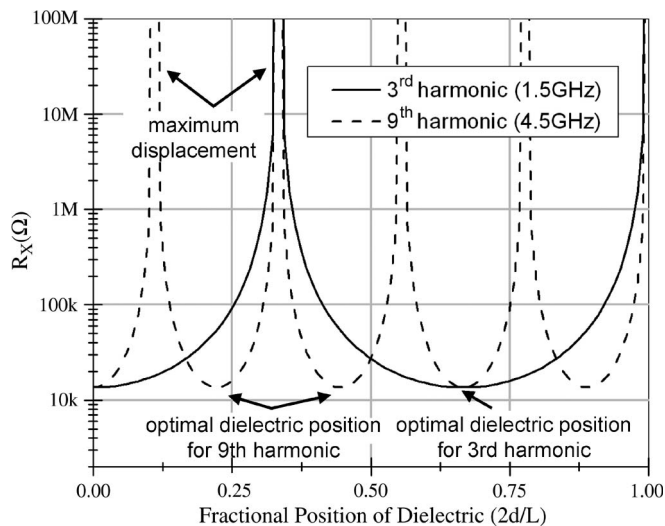
Fig. 2. R_X as a function of fractional dielectric position $|d/(L/2)|$ for the third and ninth harmonic longitudinal (width-extensional) modes of an 8.5 μm long bar. $g = 15$ nm, resonator thickness is 2.5 μm, width is 40 μm, $V_{DC} = 10$ V, $\varepsilon_f = 7\varepsilon_0$, and an $f \cdot Q$ product of 5×10^{13} is assumed.

Fig. 3. R_X scaling with frequency, normalized to the cross-sectional area of the resonator. $g = 15$ nm, $V_{DC} = 10$ V, and $\varepsilon_f = 7\varepsilon_0$. The dielectric films are placed at a maximum strain. The resonator $f \cdot Q$ product is 5×10^{13} s^{-1}.

centered at a displacement minimum or strain maximum. This choice for the position of the dielectric films sets $\cos^2(k_n d) = 1$, minimizing R_X with respect to d.

The $\sin^2$ term in the denominator of (7) results from the modal displacement at the dielectric–bulk-resonator interface. As noted in [4], this factor degrades the performance of the resonator considerably at low frequencies, where the acoustic wavelength $\lambda \gg g$. However, as the resonator scales to higher frequencies, and $\lambda/2 \to g$, the $\sin^2$ term in the denominator approaches unity, reducing motional impedance. Consequently, for a fixed dielectric thickness g determined by fabrication limitations, there is an optimal frequency of operation with acoustic wavelength $\lambda = 2 \cdot g$.

Fig. 2 shows the R_X of the third and ninth harmonics of an internally transduced longitudinal bar, varying the dielectric position along the length of the resonator. A constant $f \cdot Q$ product of 5×10^{13} is assumed for both harmonics. This value has been chosen based on observed quality factors reported in this paper. Accounting for the primary energy losses in the resonator, including Akhieser effect, thermoelastic damping, and anchor losses, the $f \cdot Q$ product is generally not a constant across all frequencies. However, this first-order approximation provides a good indication of scaling behavior.

As shown in the plot, minima in the motional impedance occur for points of maximum strain (minimum displacement). The large spatial range near the displacement minima over which R_X is low allows for fabrication of reliable devices despite misalignment tolerances. These tolerances reduce with increasing frequency as the resonant wavelength decreases, and must be considered in device design. The coincidence of displacement minima of the third and ninth harmonics at the fractional dielectric position of 2/3 allows for the optimal excitation of both modes in the same device. This may be useful for multifrequency applications. However, if multiple modes are undesired, the third harmonic can be suppressed by placing the dielectric at a fractional dielectric position of 2/9 or 4/9, near a displacement maximum of the third harmonic, while
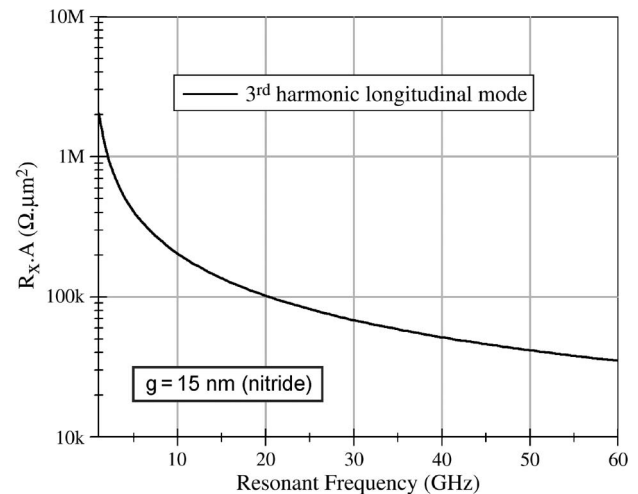
still driving the ninth harmonic at maximum strain. Conversely, placing the dielectric transducer at a fractional position of 5/9, a displacement maximum of the ninth harmonic mode, only the third harmonic will be excited, with close-to-optimal motional impedance.

Frequency scaling of the bulk-mode longitudinal resonators using internal dielectric transduction is shown in Fig. 3. The motional impedance, normalized to the cross-sectional area of the resonator, decreases drastically with increasing frequency, achieving tens of k$\Omega \cdot \mu$m^2 impedances at 60 GHz. Again, a constant $f \cdot Q$ product of 5×10^{13} is assumed. The frequency scaling result in Fig. 3 converges to an FBAR-like resonator or the Bragg reflector for a solid-mounted bulk acoustic wave resonator, stacking multiple dielectrics of thickness $\lambda/2$ between conductive layers of the same thickness. Recently, such devices have been demonstrated successfully in the 10 GHz range [5].

Common dielectrics such as silicon dioxide ($\kappa \sim 3.9$) and silicon nitride ($\kappa \sim 7$) perform reliably in films as thin as a few nanometers. For such transduction film thickness, the motional impedance is minimized at > 50 GHz but may be too high for 1–10-GHz operation. Low-impedance resonators in the radio and microwave frequency range can be achieved by using high-k dielectric materials, such as barium strontium titanate (BST). While BST films are not electrically reliable below ~ 200 nm, they exhibit a high permittivity often exceeding 300. Minimizing (7) with respect to a resonant frequency for a 200 nm dielectric film, one obtains an optimal frequency of operation at 15.8 GHz for resonators with BST dielectric transducers. Assuming an $f \cdot Q$ product of 5×10^{13} and a bias voltage of 20 V, this structure has 5 k$\Omega \cdot \mu$m^2 impedance at the third harmonic resonance.

Implementing the internal dielectric transduction, we can achieve a 50 Ω resonator at 15 GHz by stacking alternate layers of silicon and BST films to excite the thickness extensional mode. Such a resonator requires only a 10 μm $\times$ 10 μm footprint to obtain the targeted impedance. With this design, however, resonator frequency is defined by the thickness of the fabricated stack. To enable fabrication of resonators operating
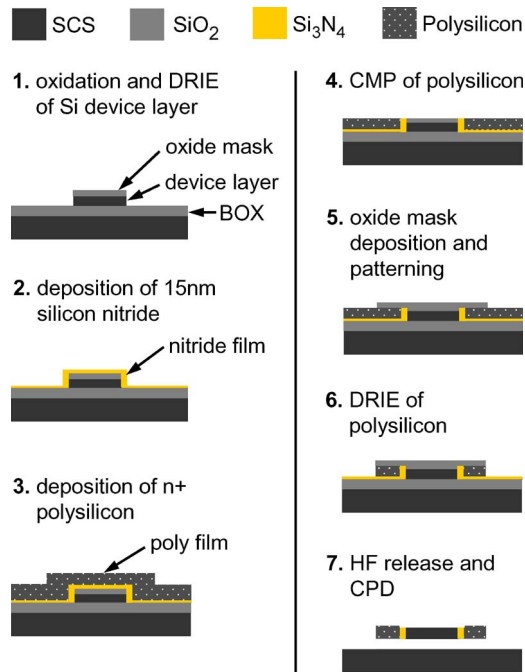
Fig. 4.   Microfabrication process for internal dielectric transduced resonators.

at various frequencies on the same chip, the resonant frequency must be defined by lithographic dimensions. With BST-based internal dielectrically transduced devices, a 50 Ω resonator can be achieved with a 1 μm thick extensional ring [6] with an approximate radius of 16 μm. This will prove to be a great advantage in obtaining low-impedance internally transduced resonators at low-gigahertz frequencies due to the large thickness of BST films.

III. FABRICATION

The resonators were fabricated in a combined SOI–polysilicon process using a 15 nm silicon nitride film for transduction, as shown in Fig. 4: 1) The device layer of a SOI wafer is first patterned in deep reactive-ion etching with a hard oxide mask, with the device layer being 2.5 μm thick; 2) a 15 nm conformal low-pressure chemical-vapor-deposition silicon nitride film is then deposited to form the transduction dielectric; 3) a layer of n+ polysilicon of > 3 μm thick is deposited and annealed; 4) the layer is smoothed with chemical mechanical polish; 5) a second hard oxide mask is then deposited and patterned; 6) the polysilicon is patterned, defining the final resonator shape; and 7) the resonators are released in an HF-timed etch followed by a critical-point dry step to prevent stiction. Although the outer rim of silicon nitride is removed in the HF release step (Fig. 5 inset), the nitride remains in the majority of the transduction area as evidenced by capacitive measurements.

Suspension beams for the resonators are designed at quarter wavelength to minimize anchor losses for both third and ninth harmonics and dampen spurious modes. The mode shape and scanning electron micrograph (SEM) of the resonator are shown in Fig. 5. As shown in the figure, the nonideal routing beams of the input and output electrodes of the resonator distort the 1-D longitudinal mode shape assumed for transduction

calculations and frequency scaling. The distorted mode, which couples an eighth harmonic surface mode to the original longitudinal resonance, slightly degrades the transduction efficiency due to a small cancellation in signal from the summed contribution of both tensile and compressive strain in the dielectric film. However, the primary contribution to the capacitive sensing results from the longitudinal component of the dielectric strain, yielding a transduction close to that described by the theory in [1].

IV. INTERNAL DIELECTRIC ACTUATION AND SENSING

A. Experimental Setup

Capacitive electromechanical resonators can be used as passive mixers due to their nonlinear electrostatic actuation. The resonator can thus be characterized by measuring the conversion loss of the mixer. A scalar-mixing measurement (Fig. 6) similar to that in [7] using an Agilent parametric network analyzer (PNA) was performed to obtain the frequency response of the resonator. A scalar-mixer calibration technique traditionally used to characterize RF mixers was implemented to measure the performance of the HF resonators. This method circumvents the capacitive losses and parasitic transmission-line resonances in the probe pads and routing of a three-port MEMS device and provides an accurate measurement of mechanical Q at frequencies well above 1 GHz [8].

Standard two-port measurements for which the input and measured frequencies are the same require deembedding structures (namely, short, open, and through structures) to cancel the parasitic capacitance, inductance, and resistance from the device measurement. In three-port scalar-mixing measurements, however, parasitic feedthrough currents occur off the resonant (measured) frequency. Since no deembedding is performed in this measurement, there exists a parasitic resistance from the probe tips to and from the device. The resistance decreases the total signal strength, resulting in an uncalibrated absolute performance of the device. The absolute R_X of the resonator cannot be extracted from the measurement without resistive deembedding and will appear higher than expected. However, for the purposes of this experiment, the absolute performance of the device is not investigated. Rather, the relative performance of the resonator operating at two different frequencies is investigated. Since the same device is probed for both harmonics and the probe tips remain fixed for the entire measurement, the resistive path from the probe tip to the device remains constant. A comparison of resonance at both harmonics, obtained without lifting the probes between measurements, therefore provides useful information about the relative transduction efficiency of the two resonant modes.

B. Results

Devices were tested at room temperature in a Lakeshore vacuum probe station, applying a 5 V bias, −10 dBm local oscillator (LO), and 0 dBm RF input. The resonator's frequency response is shown in Fig. 7. The LO leakage of the device (gray traces) was obtained by setting the bias voltage to 0 V. Acoustic resonance was excited when a 5 V bias was applied
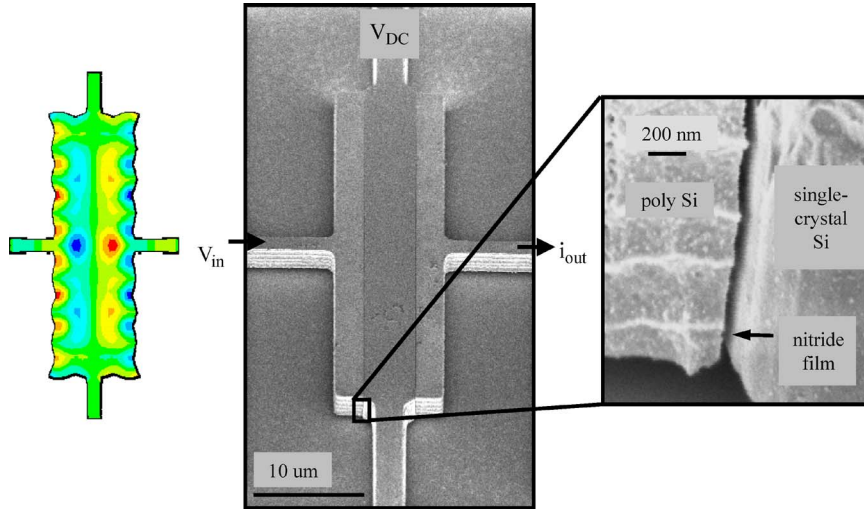
Fig. 5. (Left) Modal analysis of the third harmonic resonant mode shape of the bar resonator, simulated in Ansys. (Right) SEM of a dielectrically transduced silicon bar resonator ($8.5\ \mu$m long $\times\ 40\ \mu$m wide $\times\ 2.5\ \mu$m tall). The inset image shows the thin gap between the polysilicon and single crystal regions of the resonator.
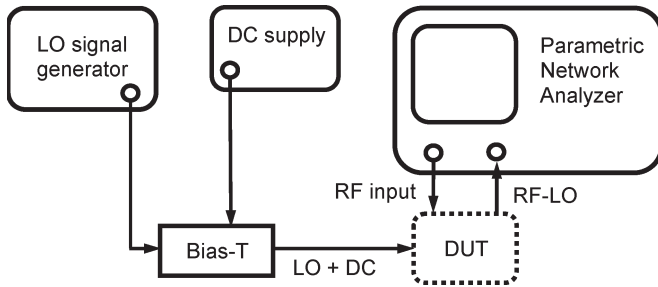

Fig. 6. Schematic of scalar-mixer measurement of the three-port MEMS resonator. The resonator (DUT) acts as a mixer for the input RF and LO signals. The resonance is detected at RF–LO, thus preventing the effects of feedthrough capacitance in the transmitted frequency response.

(black traces). The ninth harmonic, with a Q of 11 200, shows a 9.8 dB signal improvement over the third harmonic, with a Q of only 1700. The 4.51 GHz resonance has an $f \cdot Q$ product of 5.1×10^{13}.

The motional impedance in (7) is inversely proportional to Q. To extract the relationship of transducer efficiency with frequency scaling, we normalize the scalar conversion loss at resonance by the Q of the harmonic. With this normalization, we can directly compare the performance of the two harmonics. Taking this into account, the 4.51 GHz normalized signal improves by 2 dB relative to the 1.53 GHz normalized response. The analytical model predicts a $\sim 3\times$ improvement in motional impedance between the third and ninth harmonics, translating to a 4.7 dB signal improvement. The discrepancy may be due to a small misalignment (< 200 nm) and the width distortion of the longitudinal mode shape described earlier. In particular, the transducer efficiency is more sensitive to the misalignment of the dielectric film position at higher harmonics, since the misalignment corresponds to a larger fraction of the total wavelength at higher frequencies. Therefore, a misalignment in the device under test (DUT) degrades the performance of the ninth harmonic more than the third harmonic, contributing to a smaller relative transduction enhancement than expected.

V. INTERNAL DIELECTRIC ACTUATION AND PIEZORESISTIVE SENSING

A. Experimental Setup

Capacitive sensing at gigahertz frequencies is challenging due to large nominal and feedthrough capacitance intrinsic to the measurement. Three-port scalar-mixer measurements are often required. To overcome this obstacle, piezoresistive sensing of a capacitively actuated resonator is implemented [9]. There are several benefits to piezoresistive detection. Geometric and frequency scaling are considerably more favorable than in the case of capacitive sensing. In addition, independent control of the drain current enables us to set the piezoresistive transconductance g_m to be as large as possible. When a drain current I_d flows through a mechanically resonating structure, the piezoresistive change in the resistance dR/R generates a transconductance

$$g_m = \frac{dR}{R} \frac{I_d}{v_{\text{in}}} \tag{8}$$

where v_{in} is the ac voltage capacitively exciting a resonance across the dielectric films. The change in the resistance due to piezoresistivity is given as follows:

$$\frac{dR}{R} = \pi_t \sigma_t + \pi_l \sigma_l \tag{9}$$

where π_t and π_l are the transverse and longitudinal piezoresistive coefficients, and σ_t and σ_l are the transverse and longitudinal stresses, respectively. The stress is defined by the resonant mode shape with amplitude of vibrations given by (4). Summing (9) over all points in the resonator, weighting each point by the ratio of the total current density at that point to the total current density, the total fractional piezoresistive change is given by

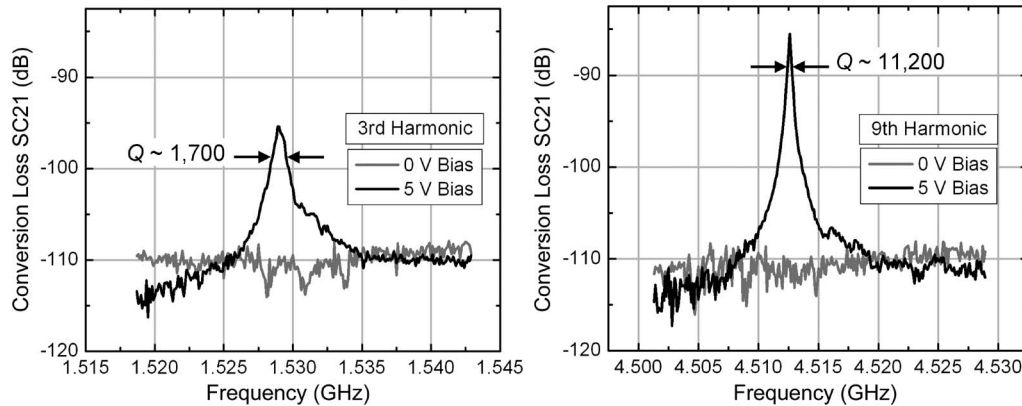$$\frac{dR}{R} = \frac{\sum_i j_i (\pi_{ti} \sigma_{ti} + \pi_{li} \sigma_{li})}{\sum_i j_i}. \tag{10}$$

Fig. 7. Measured frequency response of the third and ninth harmonic resonance of the silicon bar resonator. The gray traces (0 V) indicate the LO leakage of the device. Applying a 5 V bias excites acoustic resonance, shown in black. The ninth harmonic exhibits a 9.8 dB absolute improvement in signal strength over the third harmonic mode, with a Q increase of $6.6\times$. Normalizing the resonant peaks by Q, we extract a 2 dB enhancement of transduction efficiency in the 4.5 GHz resonance relative to the 1.5 GHz resonant mode.
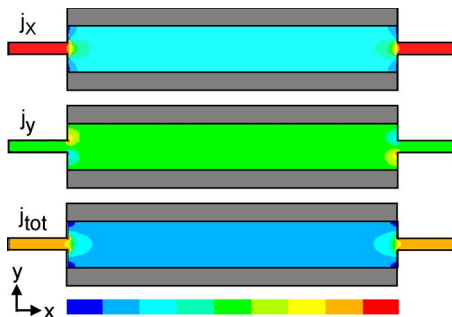

Fig. 8. Contour plot of the current density in the resonator. Current flow is uniform through most of the resonator body. Current nonuniformity at input and output of the resonator is the primary source of piezoresistive signal.
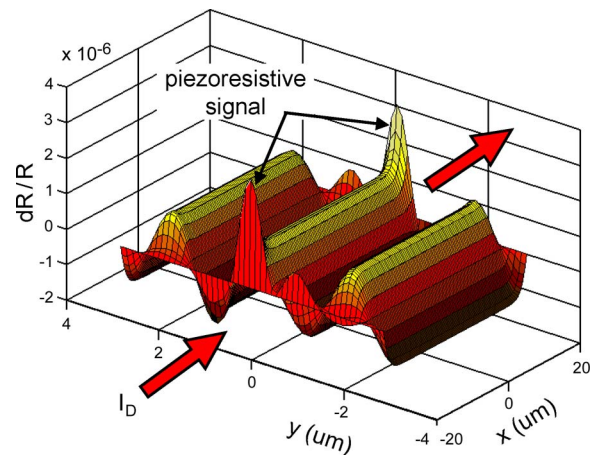

Fig. 9. Spatial distribution of piezoresistive signal. The symmetry of the strain in the resonator results in cancellation of the signal in the majority of the body. The piezoresistance peaks near the routing beams generate the detected resonant signal.

Fig. 10. Schematic of measurement setup for internal dielectric actuation and piezoresistive detection.

In the case of dielectrically actuated longitudinal-mode resonator, acoustic waves travel perpendicular to the drain current density, as shown in Fig. 8. Fig. 9 shows the analytical results of the contribution to the piezoresistive signal distributed over the resonator body, as defined by (10). The symmetry of the resonant mode and uniformity of the current flow result in a cancellation of most of the signal. With this geometry, the primary contribution to the output signal comes from vibrations in and near the suspension beams.

The ninth harmonic longitudinal resonance of the bar at 4.5 GHz was used for piezoresistive measurements. The resonator was tested at room temperature in a vacuum probe station. A schematic of the experimental setup is shown in Fig. 10. A short-open-load-through calibration on a ceramic substrate was first performed to remove parasitics up to the probe tips, followed by deembedding using short, open, and through structures on-chip. Both ends of the resonator were biased to a V_G of 10 V, and a 0 dBm (0.2 V) ac excitation from an Agilent PNA was superimposed to capacitively generate a resonance. A drain current across the resonator, defined by a bias voltage V_d, was modulated piezoresistively and detected by the PNA. The transconductance is given by subtracting the reverse transconductance (or intrinsic feedback) from the forward transconductance [10]

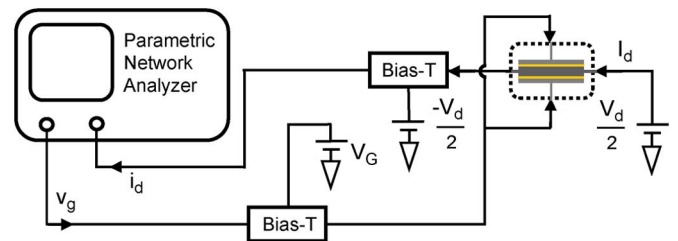$$g_m = Y_{21} - Y_{12}. \tag{11}$$

This technique is identical to microwave frequency measurement of the transconductance in transistors.

B. Results

The measured frequency response of the ninth harmonic longitudinal mode with drain currents of 1.22, 11.82, and 23 μA is shown in Fig. 11. At 23 μA, a resonant frequency of 4.41 GHz with an electromechanical Q of 8180 is observed, with a piezoresistive transconductance of 1.1 μA/V. The power dissipated in the resonator is 0.46 mW. The phase of the
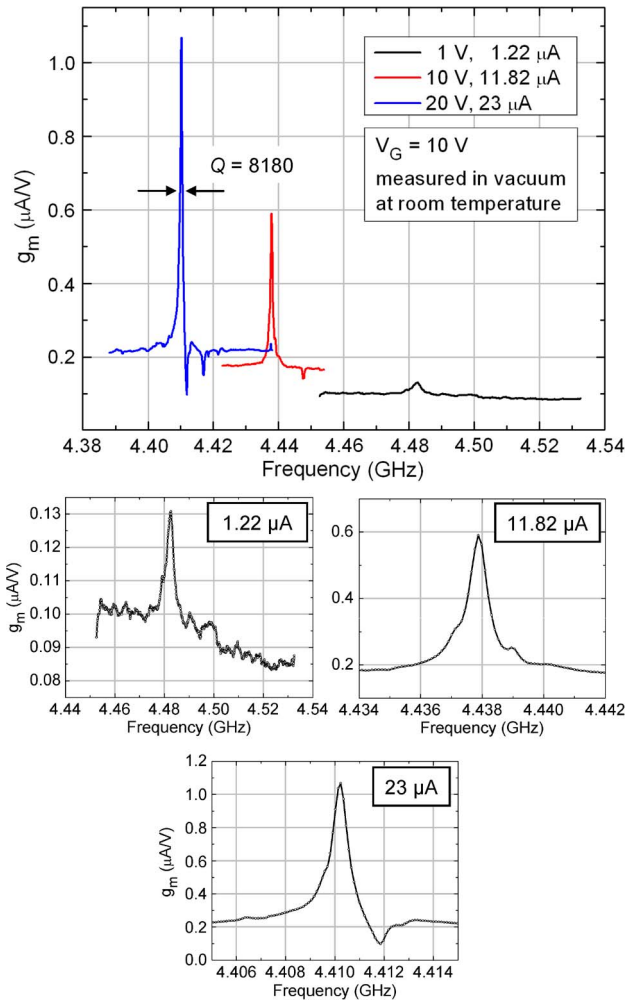
Fig. 11. Measured frequency response of transconductance g_m of the resonator for varying drain currents.

Fig. 12. Resonator phase measured across resonance with a drain current of 23 μA. The resonator makes a clear transition from $-90°$ to $90°$.

Fig. 13. Measured resonant frequency scaling with increasing drain current. Resistive heating thermally expands the resonator and alters its Young's modulus, decreasing the resonant frequency with increasing internal temperature.

Fig. 14. Measured electromechanical Q_{em} with increasing drain current.

resonator is measured across the resonance peak at a drain current of 23 μA, showing a clear transition between $-90°$ and $90°$, as shown in Fig. 12. Several trends occur as the drain current through the resonator increases. As drain current increases, the resonant frequency decreases, as shown in Fig. 13. This is due to thermal expansion and tuning of the Young's modulus of the silicon bar as a result of joule heating. A 1.6% change in frequency is observed, varying the current flow through the resonator from 1.22 to 23 μA. This frequency shift can be exploited for active frequency tuning, adjusting for the dependence of g_m on drain current using subsequent circuit stages.

Fig. 14 shows the experimental shift in electromechanical Q as the current increases. This steady-state trend is obtained after cycling the current through the resonator from low to high multiple times, allowing for desorption of molecules at the surface of the resonator through heating. The 5% variations in quality factor observed with changing drain current fall within the uncertainty of measurement. At a maximum current of 23 μA, the resonant signal exhibits an electromechanical $f \cdot Q$ product of 3.6×10^{13} s^{-1}. While the three-port scalar-mixer measurement used for capacitive sensing provides an accurate measure of the resonator's mechanical Q, the quality factor obtained in the two-po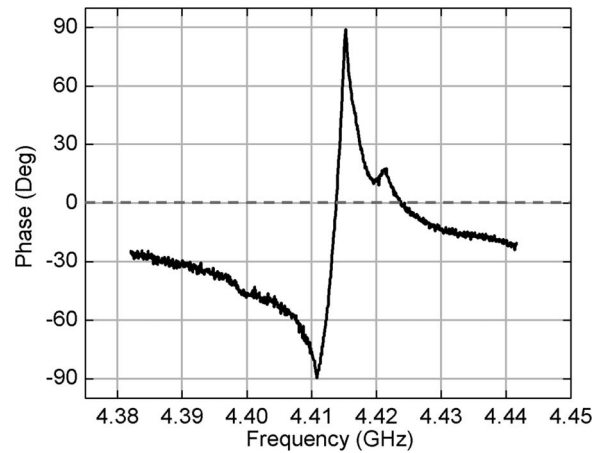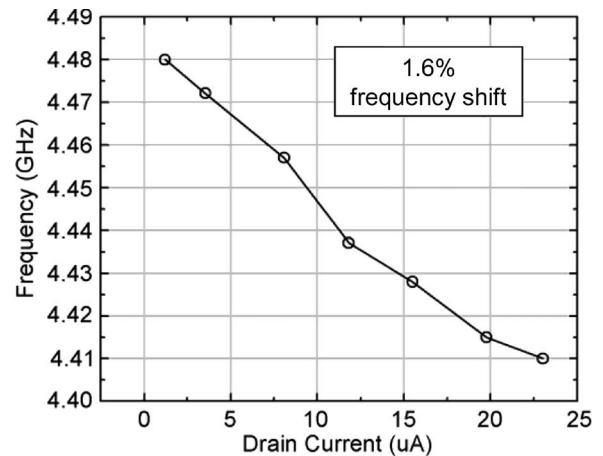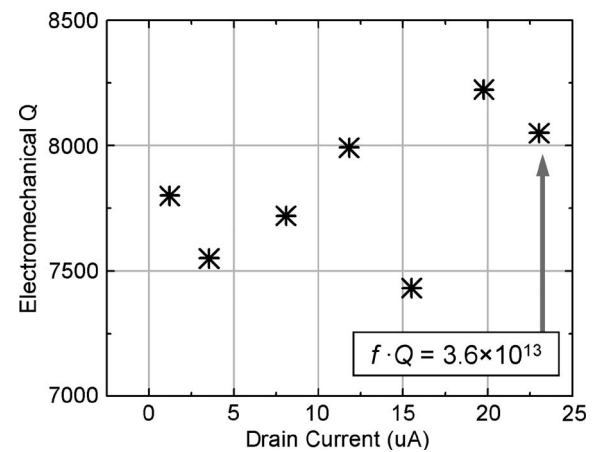rt piezoresistive measurement combines the mechanical and electrical contributions to Q, resulting in an electromechanical Q commonly quoted in the literature. This electromechanical $f \cdot Q$ product is the highest measured to date in silicon. As shown in Fig. 15, piezoresistive transconductance scales linearly with drain current, dictated by (8), with a 1.1 μS
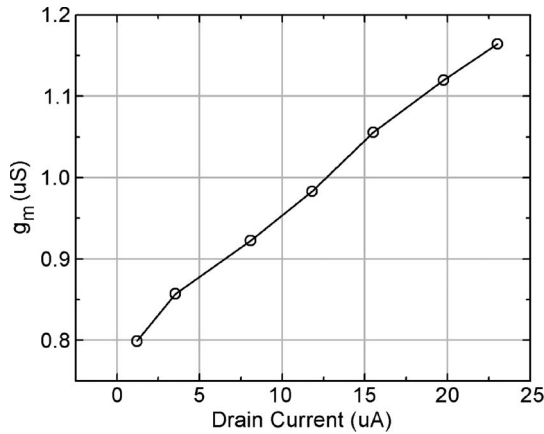
Fig. 15. Experimental resonator transconductance g_m scaling with increasing drain current.

signal at 23 μA of drain current. The extracted piezoresistive dR/R for this device is 1%.

VI. CONCLUSION

The concept of "internal dielectric transduction" has been proposed and experimentally verified. A 4.5 GHz longitudinal bar resonator is demonstrated, marking the highest frequency measured to date in silicon. The third and ninth harmonics of longitudinal vibration were excited in a silicon bar resonator, demonstrating a 9.8 dB absolute improvement in signal strength and 2 dB (Q-normalized) enhancement in transduction efficiency for the ninth harmonic (4.5 GHz) relative to the third harmonic (1.5 GHz). The 4.5 GHz resonance exhibits a mechanical $f \cdot Q$ product of 5.1×10^{13}, the highest $f \cdot Q$ product reported to date using a mixing measurement. These results indicate an improved resonator performance with increased frequency, providing a means of scaling MEMS resonators to previously unattainable frequencies in silicon (10 GHz and above).

Piezoresistive sensing was presented as a viable improvement over internal dielectric capacitive sensing in HF resonators, offering a two-port configuration to facilitate direct incorporation of RF MEMS resonators into integrated circuit applications. The measured resonance at 4.41 GHz demonstrates an electromechanical Q of 8180. The $f \cdot Q$ product of the resonator is higher than previously measured in silicon using a 3 dB direct two-port measurement, indicating the promise of internal dielectric actuation in > 1 GHz resonators. Piezoresistive sensing, which does not require a scalar-mixer measurement, yields a measurement of the electromechanical Q as opposed to a purely mechanical Q. This is the true measurement of Q used in the design of integrated devices. A power consumption of < 1 mW and control of g_m make these NEMS-transconductor hybrid resonators ideal candidates for integration into HF CMOS technology.

ACKNOWLEDGMENT

REFERENCES

[1] D. Weinstein and S. A. Bhave, "Internal dielectric transduction: Optimal position and frequency scaling," *IEEE Trans. Ultrason., Ferroelectr., Freq. Control*, vol. 54, no. 12, pp. 2696–2698, Dec. 2007.

[2] Y.-W. Lin, S.-S. Li, Y. Xie, Z. Ren, and C. T.-C. Nguyen, "Vibrating micromechanical resonators with solid dielectric capacitive transducer gaps," in *Proc. IEEE Freq. Control Symp.*, 2005, pp. 128–134.

[3] B. A. Auld, *Acoustic Fields and Waves in Solids*, 2nd ed. Malabar, FL: Kreiger Publ. Co., 1990.

[4] V. Kaajakari, A. T. Alastalo, and T. Mattila, "Electrostatic transducers for micromechanical resonators: Free space and solid dielectric," *IEEE Trans. Ultrason., Ferroelectr., Freq. Control*, vol. 53, no. 12, pp. 2484–2489, Dec. 2006.

[5] S. Gevorgian, A. Vorobiev, and T. Lewin, "DC field and temperature dependent acoustic resonances in parallel-plate capacitors based on $SrTiO_3$ and $Ba_{-0.25}Sr_{0.75}TiO_3$ films: Experiment and modeling," *J. Appl. Phys.*, vol. 99, no. 12, pp. 124 112-1–124 112-11, Jun. 2006.

[6] B. Bircumshaw, G. Liu, H. Takeuchi, T.-J. King, R. T. Howe, O. O'Reilly, and A. Pisano, "The radial bulk annular resonator: Towards a 50 Ω RF MEMS filter," in *Proc. IEEE 12th Int. Conf. Solid-State Sens., Actuators, Microsyst.*, 2003, pp. 875–878.

[7] A.-C. Wong and C. T.-C. Nguyen, "Micromechanical mixer-filters ("mixlers")," *J. Microelectromech. Syst.*, vol. 13, no. 1, pp. 100–112, Feb. 2004.

[8] Agilent Technol., Frequency Converter Application, Santa Clara, CA, Mar. 20, 2009. [Online]. Available: http://na.tm.agilent.com/pna/help/PNAWebHelp/FreqOffset/FCA.htm

[9] J. T. M. van Beek, G. J. A. M. Verheijden, G. E. J. Koops, K. L. Phan, C. van der Avoort, J. van Wingerden, D. Ernur Badaroglu, and J. J. M. Bontemps, "Scalable 1.1 GHz fundamental mode piezo-resistive silicon MEMS resonator," in *IEDM Tech. Dig.*, 2007, pp. 411–414.

[10] A. M. Niknejad, *Electromagnetics for High-Speed Analog and Digital Communication Circuits*, 1st ed. Cambridge, U.K.: Cambridge Univ. Press, 2007.

Dana Weinstein (S'05–M'09) received the B.A. degree in physics from the University of California, Berkeley, in 2004, and the Ph.D. degree in applied physics from Cornell University, Ithaca, NY, in 2009.

Since August 2009, she has been with the Massachusetts Institute of Technology, Cambridge, where she is currently an Assistant Professor in the Department of Electrical Engineering and Computer Science. She is affiliated with the Microsystems Technology Laboratories. Her research interests focus on hybrid NEMS devices, with emphasis on acoustic excitations in electron devices for millimeter-wave wireless communications, frequency sources, and sensor applications.

Prof. Weinstein was the recipient of the Olin Fellowship from Cornell University and the National Defense Science and Engineering Grant from the U.S. Department of Defense. She received the Roger A. Haken Best Paper Award at IEDM 2007.

Sunil A. Bhave (S'99–M'04) received the B.S. and Ph.D. degrees in electrical engineering and computer sciences from the University of California, Berkeley, in 1998 and 2004, respectively.

In October 2004, he joined the faculty of Cornell University, Ithaca, NY, where he is currently an Assistant Professor in the School of Electrical and Computer Engineering. His research interests focus on MEMS resonators for radio front ends, merged CMOS-NEMS for low-power computation, inertial and acoustic sensors, and hybrid photonic NEMS and magnetic NEMS for low-phase-noise microwave oscillators.

Prof. Bhave has served on the Technical Program Committees of the IEEE MEMS, IEEE International Electron Devices Meeting, IEEE International Ultrasonics Symposium, and IEEE International Frequency Control Symposium. He was the recipient of the NSF Early CAREER Development Award in 2007 and the DARPA Young Faculty Award in 2008.